

1 **Green and simple approach for low-cost bioproducts preparation and CO₂**
2 **capture**

3
4 Gabriela Durán-Jiménez^{*1}, Emily T. Kostas², Lee A. Stevens¹, Will Meredith¹, Maria Erans¹,
5 Virginia Hernández-Montoya³, Adam Buttress¹, Clement N. Uguna¹, Eleanor Binner¹

6
7 ¹Faculty of Engineering, the University of Nottingham, University Park, Nottingham, NG7
8 2RD, U.K

9 ²Department of Biochemical Engineering, University College London, Gower Street, London,
10 WC1H 6BT, UK.

11 ³TecNM/Instituto Tecnológico de Aguascalientes, Av. Adolfo López Mateos No. 1801 Ote.
12 C.P. 20256, Aguascalientes, México.

13
14 * Corresponding author

15 e-mail: Gabriela.duranjimenez1@nottingham.ac.uk

16 Tel: +44 (0)77 2793 4248

27 **Abstract**

28 This study has demonstrated, for the first time, a simple, fast and flexible microwave processing
29 method for the simultaneous preparation of bio-products (bio-oil, bio-gas and biochar) using a
30 methodology that avoids any form of catalyst or chemical activation. The dielectric properties
31 of biomass and physicochemical characterisation such as TGA, elemental and proximate
32 analysis, XRD, SEM/EDX and textural properties, showed that 8 kJ g⁻¹ of microwave energy
33 can produce superior biochars for applications in CO₂ capture. The maximum CO₂ uptake
34 capacity for biochar produced was 2.5 mmol g⁻¹ and 2.0 mmol g⁻¹ at 0 and 25 °C and 1 bar,
35 which and also exhibited high gas selectivity compared with N₂, fast kinetics of adsorption
36 (<10 min) and desirable reusability (>95 %) after 20 cycles. GC-MS analysis of generated bio-
37 oil products revealed that higher microwave energies (>8 kJ g⁻¹) significantly enhanced the
38 amount of bio-oil produced (39 %) and specifically the formation of levoglucosan, furfural and
39 phenolics compounds, and bio-gas analysis identified trace levels of H₂ and CH₄. The results
40 from this study confirm a green, inexpensive and efficient approach for biomass valorisation
41 which can easily be embedded within bio-refinery process, and also demonstrates the potential
42 of biochars for post-combustion CO₂ uptake.

43

44

45

46

47

48

49

50

51 **KEYWORDS: Lignocellulosic Biomass, Microwave pyrolysis, Bio-oil, Biochar, CO₂**
52 **capture**

53 1 Introduction

54 The issues regarding climate change have attracted considerable attention, particularly since
55 the average global temperature has been estimated to increase due to the greenhouse gas
56 emissions. In 2011, the European Union reaffirmed its objective to reduce carbon dioxide
57 (CO₂) emissions by 80-90 % (“Nations, U. Paris Agreement to the United Nations Framework
58 Convention on Climate Change,” 2015)(Zappa et al., 2019). In order to achieve these goals,
59 research efforts have focussed on the sustainable valorisation of biomass feedstocks and their
60 conversion into energy, fuels and bio-products; with emphasis on processes that can reduce
61 emissions and promotes circular bio-economy (Acevedo-García et al., 2020)(Olabi, 2019).

62 The transformation of biomass residues to chemicals has the potential to produce bio-products
63 base for bio-refinery, adhesives, surfactants and plasticisers using technologies such as
64 fermentation, extraction, hydrolysis, gasification and pyrolysis. In this sense, it is estimated
65 that more than 422,800 tons of pecan nut shell (NS) (*Carya illinoensis*) are produced yearly,
66 representing a significant volume of waste available for the generation of added value bio-
67 products (Agustin-Salazar et al., 2018). Recent reports highlight its use for the preparation of
68 reduced sugars (Santos et al., 2020), as reinforcing filler in poly (lactic acid) biocomposites
69 (Agustin-Salazar et al., 2018), gasification for syngas generation (Aldana et al., 2015) (Lozano
70 and Lozano, 2018) and as precursor of adsorbent for energy storage (Martínez-Casillas et al.,
71 2019).

72 Amongst the available thermochemical processes, microwave pyrolysis has proved to be a very
73 attractive processing technology, due to its nature and volumetric heating which offers the
74 possibility to heat selectively and therefore maximize the production of desired products
75 (Durán-Jiménez et al., 2015)(Kostas et al., 2020)(Kostas et al., 2017)(Beneroso et al., 2017).
76 The heating effect resulting from the interaction of microwave energy with biomass

77 predominantly occurs through coupling of both permanent and induced dipoles, as well as ionic
78 components of the material to the oscillating electromagnetic field. This motion then induces
79 molecular friction and generation of heat within the volume of the material (Kostas et al., 2019).
80 The energy is transferred from inside to outside of the particle which results in an inverted
81 temperature gradient (Haeldermans et al., 2019)(Kostas et al., 2017). Compared with
82 conventional heating, this technology offers a variety of advantages, such as greener
83 instantaneous heating and the elimination of catalyst or other auxiliary chemicals, which means
84 that wastes are not generated (Durán-Jiménez et al., 2020)(Yin, 2012). By the evaluation of
85 dielectric properties, microwave have proved to be compatible with biomass feedstock
86 pyrolysis processes to generate a range of bio-based products including bio-oils and biochars
87 (Kostas et al., 2019)(Yin, 2012)(J. Li et al., 2016)(Kostas et al., 2020)(Sears et al.,
88 2006)(Durán-Jiménez et al., 2016)(Ferrera-Lorenzo et al., 2014). Bio-oils typically contain a
89 mixture of oxygenated compounds (Kan et al., 2016), and have the potential to be catalytically
90 upgraded to fuel. Biochar is a porous carbon-based material used in several applications
91 including batteries, catalyst, soil remediation and as adsorbent of pollutants in liquid and gas
92 systems (Li et al., 2017)(Kan et al., 2016).

93 Nowadays, several materials such as fly ashes (Bui Viet et al., 2020) biomass, cement kiln dust,
94 paper sludge, sewage sludge (Sanna et al., 2012), activated carbons (Srinivas et al.,
95 2014)(Hoseinzadeh Hesas et al., 2015)(Yang et al., 2017), zeolites and metal organic
96 frameworks (Lin et al., 2014)(Liang et al., 2009)(Saha et al., 2010) have been investigated for
97 CO₂ capture. Particular interest in the preparation of biochar for CO₂ capture has also been
98 reported due to its simplicity and low cost (Huang et al., 2015). However, research has focused
99 on the modification of biochar by chemical and physical activation (Li and Xiao, 2019)(Y. Li
100 et al., 2016)(C. Zhang et al., 2016) or the incorporation of metals into the skeleton of biochars
101 (Lahijani et al., 2018) to enhance their CO₂ adsorption capacity. This modification has resulted

102 in the increase of the costs and difficulties in the regeneration limiting its industrial application.

103 Currently, there is a huge need in the study of more environmentally friendly processes for the
104 synthesis of biochars with effective adsorption properties. However, the global biomass
105 valorisation (liquid, solid and gas fraction) and the detailed assessment of CO₂ adsorption
106 capacities of biochars obtained without chemical modification and microwave heating, have
107 not been evaluated. The conversion of waste biomass feedstocks into added-value products will
108 address issues related to its disposal, which is essential for a sustainable global circular bio-
109 economy (Acevedo-García et al., 2020). Furthermore, the application of products generated in
110 one step that also avoids the use of catalysts is highly appealing from an environmental and
111 energy consumption perspective.

112 To our knowledge, this is the first study that employs nut shell as a renewable source that
113 complies within a bio-refinery setting for multiple generation of added value products. This
114 study does not only focus on the characterisation of generated bio-oil from microwave
115 pyrolysis process, but also in the application of biochar. A detailed discussion of the
116 physicochemical characterisation and evaluation of the simple-to-produce biochars for post-
117 combustion CO₂ capture is presented, with assessments focussing on the kinetics, selectivity,
118 reusability and equilibrium of adsorption of CO₂ at relevant temperatures (0 and 25 °C).

119 **2 Materials and methods**

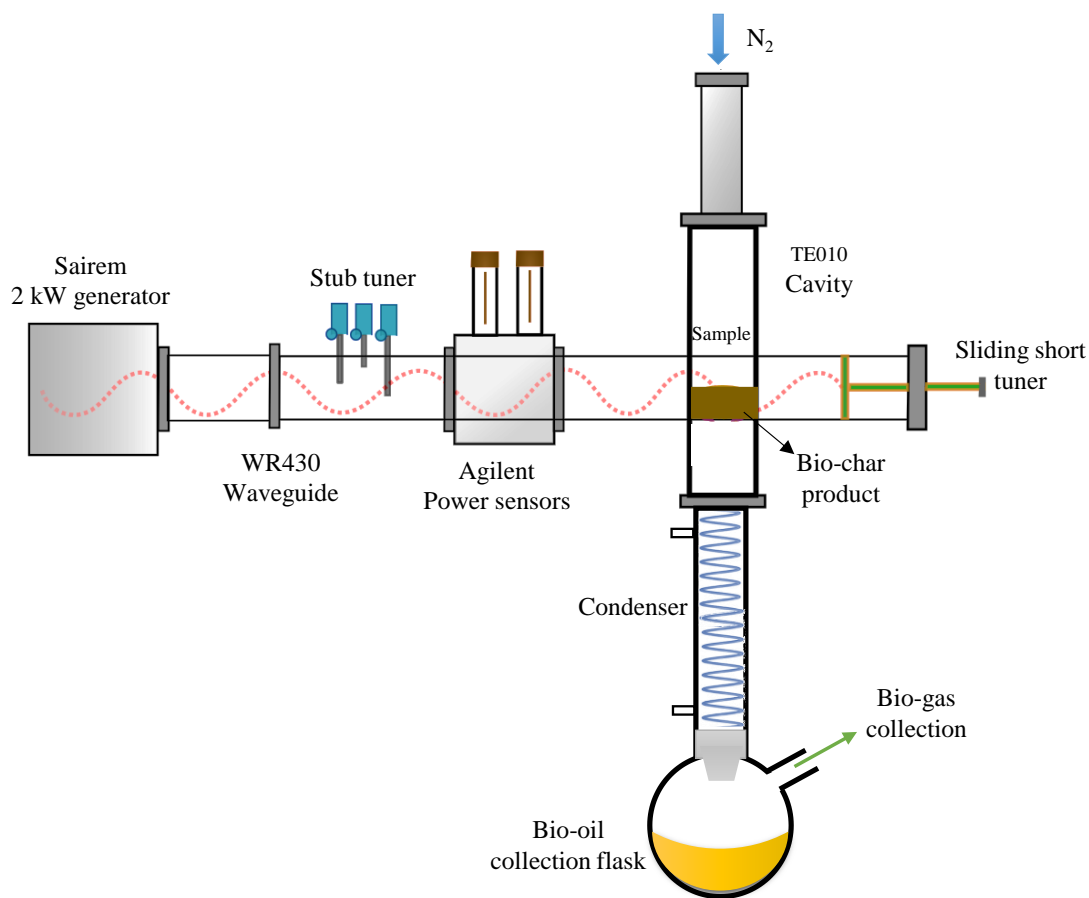
120 **2.1 Materials**

121 In this study pecan nut shell (NS) was used as raw material. Prior to pyrolysis experiments, NS
122 was washed and dried at 70 °C.

123 **2.2 Biomass pyrolysis experiments**

124 The system used in the microwave pyrolysis is shown in Fig. 1, and is composed by one mode

125 applicator, 2 kW microwave generator (2.45 GHz), an automatic tuner (S-TEAM STHD v1.5)
126 and sliding short to maximise the power density in the sample. (Durán-Jiménez et al., 2020).
127 The sample was placed in a quartz reactor in nitrogen atmosphere (2 L min^{-1}).
128 The microwave processing conditions were in the range of 300-400 W input power and 2 to 6
129 min duration time as shown in Table S1. The liquid fraction was stored in a pre-weighed vials
130 at $4 \text{ }^{\circ}\text{C}$. The non-condensable gases were passed into a gas line and collected using a tedlar gas
131 bag for subsequent analysis.



132

133 Fig. 1. Microwave pyrolysis system used in this work

134 It should be noted that it is unfeasible to accurately measure the sample temperature as
135 microwave heating causes volumetric and instantaneous heating (Nagahata and Takeuchi,
136 2019).

137 The biochar and bio oil yield were quantified by their weights and the yield of the non-
138 condensable product was calculated by difference as follow:

139
$$Y_{Bio-char} = \frac{M_{Bio-char}}{M_0} \times 100 \quad (1)$$

140
$$Y_{Bio-oil} = \frac{M_{Bio-oil}}{M_0} \times 100 \quad (2)$$

141
$$Y_{Bio-gas} = 100 - [Y_{Bio-char} + Y_{Bio-oil}] \quad (3)$$

142

143 **2.3 Characterisation techniques**

144 **2.3.1 Dielectric properties**

145 The dielectric response of a material is commonly presented as permittivity (ϵ) which can be
146 given by:

147
$$\epsilon = \epsilon_0 \epsilon_r = (\epsilon_r' - j\epsilon_r'') \quad (4)$$

148 where ϵ_0 is permittivity of the free space (8.854×10^{-12} F m⁻¹), ϵ_r is complex relative
149 permittivity, and j is imaginary unit ($j^2 = -1$). The complex relative permittivity is composed by
150 the real part, called relative dielectric constant (ϵ_r'), and it is a measure of the ability of the
151 material to store electrical energy; and the imaginary part, (ϵ_r'') known as relative dielectric loss
152 factor, represents the energy dissipated. Dielectric properties of NS were obtained using the
153 cavity perturbation technique for a temperature range of 20 - 650 °C at 2450 MHz (Durán-
154 Jiménez et al., 2020). The sample was placed in the system using a quartz tube of (ID) 3 mm
155 that is moved by an automated motor to the furnace and cylindrical TM_{0n0} mode cavity. The
156 dielectric properties were calculated using the cavity response between a load and empty tube
157 measured by a HP 8753 vector network analyzer (VNA). The results presented in this work are
158 the averages of 3 replications.

159 **2.3.2 Bio-gas and Bio-oil Analysis**

160 The bio-gas generated during the pyrolysis experiments were analysed as described somewhere
161 else (Almustapha et al., 2017), using a Clarus 580 Gas Chromatograph (GC) system.

162 The bio-oil were analysed by GC-MS using a Varian CP-3800 GC incorporated to a Varian
163 1200 MS (70 eV, EI mode) (Kostas et al., 2019). The identification of the compounds in the
164 bio-oils was determined according to the NIST Mass Spectral library from the National
165 Institute of Standards and Technology, Maryland, USA.

166 **2.3.3 Biochar and NS characterisation**

167 Proximate analysis was conducted by the method previously described by Donahue (Donahue
168 and Rais, 2009). The sample was placed in TGA Q500 TA Instrument and heated to 900 °C
169 under a N₂ atmosphere (100 ml min⁻¹, 1 bar) and then held at 900 °C for 15 min, the atmosphere
170 was then switched to air and held for a further 15 min. The ultimate analysis was determined
171 using a LECO CHN-628 elemental analyzer. A Philips XL 30 microscope was used to analyze
172 the morphology and the X-ray diffractograms were obtained by using a Bruker D8 Advance
173 Da Vinci.

174 The textural parameters were calculated from the N₂ adsorption isotherms at -196 °C using a
175 Micromeritics ASAP 2420 apparatus. Brunauer–Emmett–Teller (BET) theory was used to
176 calculate the surface area while the micropore, total pore volume and size distributions were
177 determined by Non-Local Density Functional Theory (NLDFT) (Thommes et al., 2015)
178 (Thommes, M., Kaneko, K., Neimark, A. V., 2015)(Thommes, M., Kaneko, K., Neimark, A.
179 V., 2015)(Thommes, M., Kaneko, K., Neimark, A. V., 2015)[42](Thommes, M., Kaneko, K.,
180 Neimark, A. V. 2015)(Thommes, M., Kaneko, K., Neimark, A. V., 2015)(Thommes, M.,
181 Kaneko, K., Neimark, A. V., 2015)(Thommes, M., Kaneko, K., Neimark, A. V.,
182 2015)(Adeniran et al., 2014) by combining a CO₂ adsorption isotherm at 0 °C to a N₂
183 adsorption isotherm.

184 **2.4 CO₂ capture experiments**

185 The CO₂ uptake of the generated biochars were determined by thermogravimetric and

186 volumetric analysis. The volumetric experiments were conducted in a Micromeritics ASAP
187 2420 analyser, where approximately 500 mg of biochar was degassed at 120 °C in N₂ for 15 h.
188 The amount of CO₂ adsorbed was determined using 100 % CO₂ in the range of 0.001 to 1.2
189 bar. The thermogravimetric uptake was performed using a TGA Q500 TA instrument.
190 Approximately 25 mg of biochar was placed in a pan and dried for 30 min at 120 °C and
191 atmospheric pressure. After the physisorbed moisture was removed, the sample was cooled
192 down to 25 °C and the gas was switched at 100% CO₂. Once the adsorption reached
193 equilibrium, the adsorbed amount of CO₂ was recorded vs time for 60 min, then the sample
194 was heated up to 120 °C in N₂ for 15 min to complete the CO₂ desorption. In total, 20
195 adsorption-desorption cycles were conducted to determine stability and recyclability of the
196 biochar. The selectivity was determined by thermogravimetric analysis at 25 °C using N₂ (100
197 ml min⁻¹) for the adsorption stage and Ar in the desorption stage. All experiments were
198 performed in triplicate and the averages are presented. In general, standard deviations were
199 below 5 % of average values.

200 **3 Results and Discussion**

201 **3.1 Microwave pyrolysis and bio-product formation mechanism**

202 The TG and DTG curves obtained from the pecan NS and the dielectric characterisation are
203 shown in Fig. 2. Based on the thermograms, the decomposition of the biomass occurs in three
204 main stages. The first stage involves the removal of water at temperatures up to 150 °C,
205 whereas the second and third stages describe the hemicellulose and cellulose decomposition
206 (up to 400 °C), and the lignin transformation into char (beyond 400 °C).

207 In microwave heating, the dielectric constant and loss factor determine the capability of the
208 biomass to be heated by microwave heating. The results of dielectric characterisation illustrate
209 that at temperatures below 150 °C, is the water the main responsible for the microwave

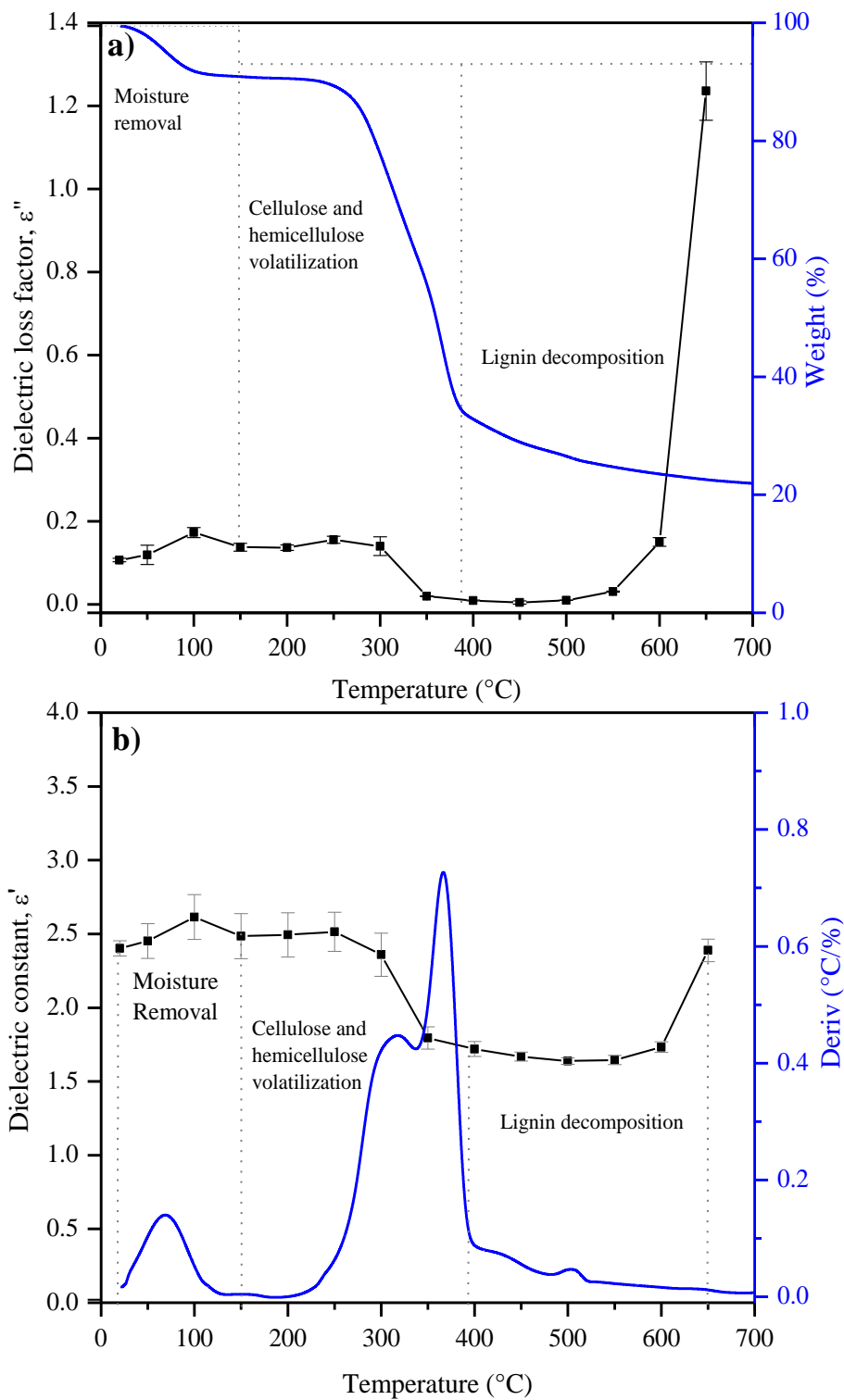
210 absorption due to dipolar mechanisms. When the water is removed the dipolar movements
211 decreased leading to the reduction the dielectric constant and loss factor. However, at
212 temperatures above 600 °C the formation of char is promoted and hence an exponential
213 increase in the dielectric properties is observed, as results of the increase in the conductivity of
214 the sample. Similar behaviour for lignocellulosic biomasses have been previously reported
215 (Miura et al., 2004)(Namazi et al., 2015).

216 The distribution of the three pyrogenic products generated from the pyrolysis of NS using
217 microwave heating, are presented in Table S1. The yields of biochar are in the range of 16 –
218 18 %. It has been reported the bio-oil yields for lignocellulosic biomasses such as pine wood
219 and corn stover ranges between 20- 40 % (Kan et al., 2016) (Jung et al., 2019). Similar yields
220 were found in this study (21.5 - 40 %).

221 The results indicate the higher bio-oil yields are a result of the faster processing times achieved
222 in microwaves, and also confirm that microwave pyrolysis could be thermochemically faster
223 than slow pyrolysis in a conventionally heated process (Huang et al., 2015). The bio-oil yields
224 were correlated to the specific energy, which is a measure of the real absorbed energy by the
225 sample under processing. It appeared that at higher energies but low intensities (300 W) is
226 possible to obtain higher bio-oil yields, which can be as result of a more controlled volatile
227 matter evolution in the pyrolysis process. For example, the samples prepared at 300 W showed
228 a positive trend where the highest bio-oil yield (39.0%) corresponds to the higher specific
229 energy (8 kJ g⁻¹). This behaviour, was different for bio-oils produced using incident power of
230 400 W where the yield decreased for samples prepared at higher energy (24.8% at 8.4 kJ g⁻¹)
231 This phenomena can be explained in terms of heating rate and power density. For samples IV-
232 N (300 W - 6 min) and VII-NS (400 W – 4 min), similar specific energy was reported, however
233 in VII-NS the heating rate and power density were higher, leading to the preferred gas
234 production and lower bio-oil yields.

235 This study confirms that the NS bio-oil yield is highly governed for the energy, but also for the
236 power density used in the pyrolysis. This is of great relevance and establish the basis for
237 microwave processing where the maximisation of bio-oil is priority.

238 The complex transformation of biomass into biochar and bio-oil has been proposed as result of
239 several depolymerisation reactions. The model describes groups in cellulose and hemicellulose
240 such as glucomannans and containing glycosidic bond that broke down to into levoglucosan
241 that further undergoes dehydration and intramolecular arrays to produce furfural and furan
242 (Singh et al., 2019). Lignin is a complex cross- linked polysaccharide and its decomposition
243 results in the formation of the biochar network (J. Li et al., 2016). The polymerisation and
244 aromatisation mechanisms produce the formation of wide-range phenols in the liquid phase
245 and rich carbon content solid (biochar).



246

247 Fig. 2. Dielectric properties and TGA (a) & DTG (b) pecan NS as a function of temperature

248 **3.2 Bio-oil and bio-gas characterisation**

249 The most prominent compounds identified in bio-oils were semi-quantitatively analysed and

250 are shown in Table 1. Fig. 3 illustrates a typical GC-MS total ion chromatogram, and all
251 samples are shown in Fig. S1. It can be seen that bio-oils are a mixture of numerous organic
252 compounds that have resulted from the pyrolytic breakdown of lignin, cellulose and
253 hemicellulose as per in Fig. S2, which include water, vanillins, furan carboxaldehydes,
254 pyrones, acetic acid, hydroxy-aldehydes and phenolics. A range of phenolic based compounds
255 such as methoxyphenol, dimethylphenol, ethylmethoxyphenol, methoxyvinylphenol,
256 methoxypropenylphenol were detected with totalling concentrations ranging between 28 to
257 44.5 % of the identified compounds. The presence of the aforementioned phenol derivatives
258 have resulted from the depolymerisation of lignin and its monomeric constituents, which
259 according with the TGA analysis in Fig. 2, typically occur at temperatures between 400 and
260 600 °C (Mohan et al., 2006). Phenolic compounds can be used in the synthesis of bio-plastics,
261 resins and epoxy polyurethane materials (Mamaeva et al., 2016).

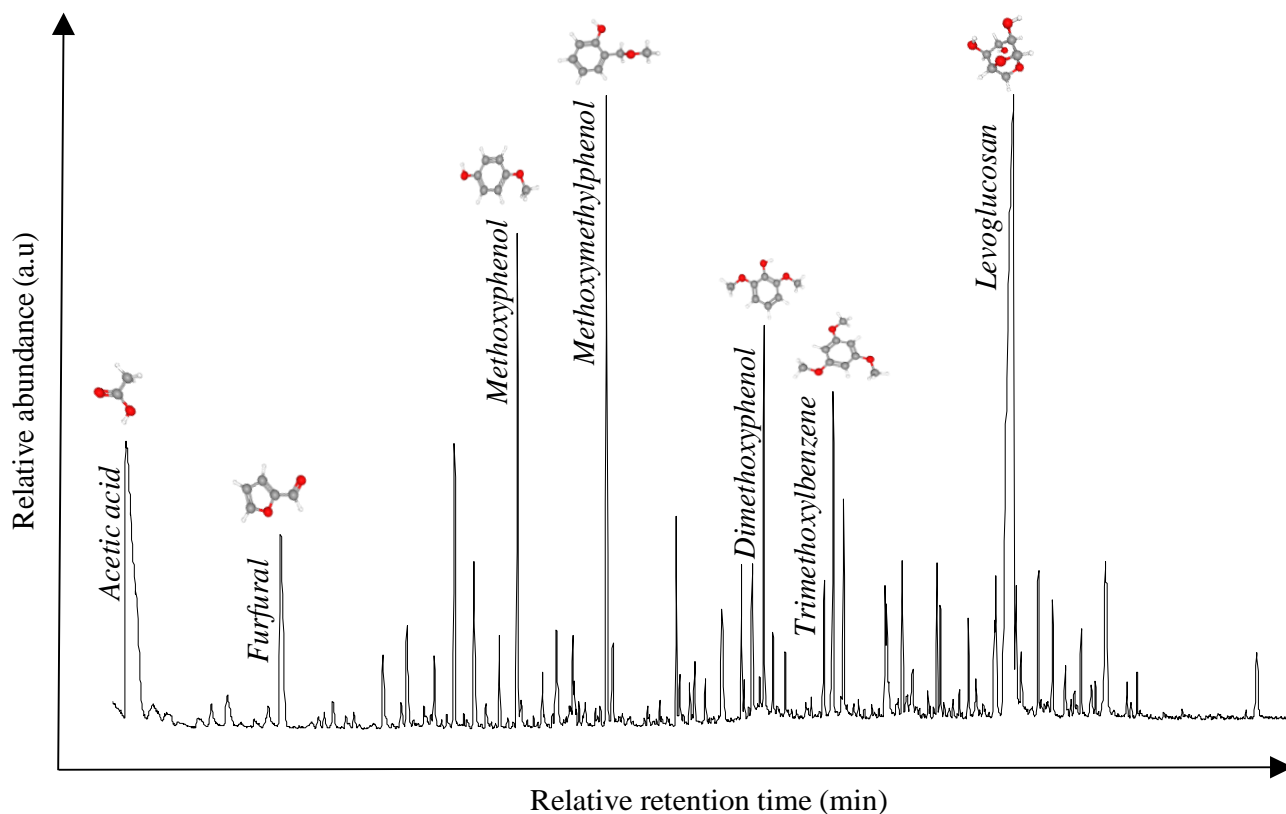
262 Cellulose degradation is expected to occur at lower temperatures (usually between 240 - 350
263 °C) and results in the formation of anhydrocellulose and levoglucosan (Mohan et al.,
264 2006)(Kostas et al., 2020)(Wu et al., 2009). Around 8.6 – 23.1 % of the total compounds
265 identified in the generated bio-oils from this study was indeed levoglucosan, representing a
266 valuable precursor fraction for conversion into plastics, surfactants, and bio-polymers (Rover
267 et al., 2019). On the contrary, the main monomeric products from hemicellulose decomposition
268 led to the formation of furfural and acetic acids, ranging between 13.2 to 25.2 %. Other
269 compounds present in the bio-oils were aldehydes (6.5 – 12.4 %), methyl, vanillins and benzene
270 and its derivatives (21.3 – 29.3 %).

271 Overall, the range of compounds identified in the bio-oil fractions generated in this study are
272 comparable to bio-oils typically generated from lignocellulosic feedstock materials, offering
273 wide opportunity for upgrading and incorporation bio-product manufacture (Pinheiro Pires et
274 al., 2019).

Table 1. Semi-quantitative bio-oils composition of NS biomass.

Compound	Retention Time (min)	Percent of total identified (%)						
		I-N [300-3]	II-N [300-4]	III-N [300-5]	IV-N [300-6]	V-N [400-2]	VI-N [400-3]	VII-N [400-4]
Acetic acid	7.60	4.91	6.28	2.93	5.65	8.69	5.76	13.23
Furfural	12.64	8.28	6.99	4.47	8.18	13.47	11.48	11.95
Cyclopentanedione	15.99	1.30	1.32	1.36	1.27	1.27	1.23	1.49
Furanone	17.67	1.33	1.45	1.38	1.37	1.85	1.41	1.48
Oxazolidine, 2,2-diethyl-3-methyl-	18.34	5.04	4.58	5.50	4.69	5.88	5.35	7.98
Cyclopentanedione	18.97	3.46	2.98	2.95	2.99	3.68	3.10	3.44
Phenol	19.81	1.30	1.38	1.61	1.70	2.53	2.08	2.68
Methoxyphenol	20.40	7.87	5.23	5.42	4.64	5.68	4.94	6.66
Methylphenol	22.22	1.36	0.70	0.78	0.94	1.23	1.12	1.42
Methoxymethylphenol	23.33	9.85	6.39	7.66	6.14	6.81	6.57	8.09
Dimethylphenol	23.51	1.42	1.37	1.74	1.27	1.54	1.17	1.60
Ethylmethoxyphenol	25.62	2.75	1.45	1.76	0.32	0.40	1.57	1.77
Methoxyvinylphenol	27.10	2.86	2.19	3.16	3.04	2.81	3.20	3.42
Methoxypropenylphenol	27.77	2.09	1.26	1.46	1.28	1.40	1.42	1.70
Hydroxymethylfurancarboxaldehyde	28.11	3.13	1.88	2.41	2.04	2.59	2.01	2.48
Dimethoxyphenol	28.49	6.16	3.67	5.01	3.70	4.25	3.67	3.98
Methoxypropenylphenol	29.19	1.04	0.58	0.83	0.73	0.63	0.82	0.57
Methoxypropenylphenol	30.46	2.25	1.50	2.76	2.61	2.15	2.81	1.71
Trimethoxybenzene	30.76	4.85	2.31	4.67	4.27	3.04	4.12	2.80
Vanillin	31.10	3.50	1.93	2.54	2.15	3.20	2.39	2.37
Methoxypropylphenol	32.47	1.93	1.01	1.42	1.05	0.64	0.11	0.74
Methyltrimethoxybenzene	32.52	1.49	1.12	1.82	1.23	1.11	1.16	0.85
Hydroxymethoxyphenyl	33.03	2.02	1.13	1.62	1.22	1.58	1.29	1.16
Hydroxymethoxyphenylpropanone	34.17	1.96	0.86	1.23	0.88	0.97	0.82	0.64
Dimethoxypropenylphenol	34.29	1.69	1.00	1.39	1.22	1.33	1.16	0.83
Hydroxymethoxyphenylpropanone	35.20	1.41	0.75	1.02	0.78	0.79	0.79	0.22
Levogluconan	36.50	2.28	32.12	19.68	15.69	10.41	9.91	8.61
Dimethoxypropenylphenol	36.76	1.96	1.01	2.50	10.89	1.53	12.16	1.27
Hydroxydimethoxybenzaldehyde	37.49	2.10	1.32	1.91	1.57	1.80	1.46	1.19
Hydroxydimethoxyethanone	38.90	1.25	0.79	1.14	0.85	0.96	0.76	0.61
Hydroxymethoxycinnanaldehyde	39.70	5.52	2.83	4.58	4.35	4.10	3.00	2.39
Dimethoxyhydroxycinnanaldehyde	44.66	1.64	0.62	1.30	1.29	1.68	1.16	0.68

277 *Preparation conditions [Power (W)-time (min)]



280

281 Fig. 3. GC-MS total ion chromatogram of a bio-oil sample (I-N) [300W-2min] generated

282 from pecan NS microwave pyrolysis in this study.

283 Although the synthesis of bio-gas is beyond the scope of this work, attempts were made to

284 analyse the non-condensable fraction obtained from the pyrolysis of biomass and it was found

285 trace amounts of hydrogen (H_2) and methane (CH_4) (Fig. S3). Reasons for the trace levels could

286 be due to the fact non catalyst were used in the process to maximize the bio-gas production

287 (Weihong et al., 2019), but also due to that a relatively high nitrogen gas flow was applied in

288 order to maintain an oxygen-free atmosphere and therefore aimed the dilution of gases

289 produced. Despite the synthesis of bio-gas was not the main objective of this study, is important

290 to highlight that studies have demonstrated the potential of NS for syngas production (Aldana

291 et al., 2015), confirming the versatility and opportunities that this biomass offers for its

292 valorisation.

293 3.3 Biochar characterisation

294 The elemental composition of the generated biochar samples is presented in Table 2, and show
295 that regardless of the experimental conditions that were applied for the preparation of the
296 biochars, biomass conversion into biochar was fully achieved as indicated by the carbon
297 content ranging between 83.1 to 91.27 %. The hydrogen content (0.12 - 0.99 %), is associated
298 with the small portion of compounds which remained in the solid carbon matrix. The biochars
299 produced contained a high number of aromatic groups and relatively small aliphatic chains as
300 indicated by a low H/C ratio, confirming that the aromaticity is due to dehydration,
301 decarboxylation and cyclization reactions (Coromina et al., 2015). For all biochar samples, the
302 carbon content increased for samples prepared at higher energies, for example VII-N has a
303 specific energy of 8.4 kJ g⁻¹ and a carbon content of 91.3 %, suggesting a higher level of
304 graphitisation (See Tables 1 and 3).

305 The thermogravimetric profiles (TGA) of biochars are illustrated in Fig. S4. The weight losses
306 observed from room temperature up to 110° C, are as result of the moisture removal. From 110
307 ° C all biochars showed a weight loss due to the volatile matter degradation. The proximate
308 analysis is summarised in Table 2. The pecan NS has fixed carbon (10.8 %), volatile matter
309 (84.4 %), moisture (3.6 %) and ash (1.3 %) (Durán-Jiménez et al., 2017). For the biochar, the
310 data reveals a significant increase in fixed carbon whereas the volatile content shows a reversed
311 trend. An increase in the microwave pyrolysis energy led to an increasing conversion to char,
312 and reduction in the volatile matter. The increases observed in the fixed carbon and ash content
313 as the pyrolysis energy increases could be due to the high temperature reached in the pyrolysis.
314 The ash contents of the biochars were between 2.75 and 3.78 % and are a result of the
315 transformation of the calcium oxalate in the precursor.

316 The elemental composition of biochar samples is consistent with the powder XRD patterns

317 shown in Fig. S5. An apparent increase in the intensity can be observed for the peaks at $2\theta =$
318 23° and $2\theta = 43^\circ$. Both peaks are ascribed to the diffraction of graphitic carbon domains (002)
319 and (101) (Lahijani et al., 2018). The wide peak at 23° is associated with the highly disordered
320 structure or amorphous carbon. The peak at $2\theta = 43^\circ$ correspond to the spacing between
321 aromatic layers (Serafin et al., 2019). Additionally, the pecan NS biomass is rich in calcium in
322 the form of oxalates ($\text{CaC}_2\text{O}_4 \cdot \text{H}_2\text{O}$), which progressively disappeared at higher microwave
323 energy and at the time new peaks of CaCO_3 were formed in the biochar. This behaviour can be
324 due to higher energies promote the decomposition of the oxalates, which is expected to occur
325 at temperatures beyond 450°C .

326 The morphology of the biochar prepared using a microwave power of 300 W for 6 min (IV-N)
327 was analysed by SEM (Fig. S6 5 a-b) and EDX (Figs. S6 c-d). The morphology shows irregular
328 cavities and pores (Fig. S6 a-b). The electron diffraction illustrates that the presence of
329 superficial deposits composed of CaCO_3 (Fig. S6 c). The composition is validated by the XRD
330 analysis (Fig. S5 b).

331 The textural parameters and the N_2 adsorption isotherms at -196°C presented in Table 2 and
332 Fig. S7. In general, the temperature required to devolatilise the biomass was successfully
333 achieved after 3 min, thus enhancing the surface area and porosity of the biochar, whereas the
334 largest specific surface area ($187 \text{ m}^2 \text{ g}^{-1}$) and the highest pore volume ($0.075 \text{ cm}^3 \text{ g}^{-1}$) were
335 observed in the biochar prepared at 300 W for 6 min (300W -6 min). The results suggest that
336 by increasing the microwave processing time to 6 min, the degree of micropore fraction also
337 increases (85 %). The reduction in specific surface area and development of micropores along
338 with the increase of specific energies (beyond 8 kJ g^{-1}), can be related to the disintegration of
339 porous cavities as they are exposed to higher temperatures. Similar results have been previously
340 reported for biochar prepared from similar biomass feedstocks such as walnut shells (Lahijani
341 et al., 2018).

342 All biochars prepared exhibited a type I isotherm based on the IUPAC classification
343 (Thommes, M., Kaneko, K., Neimark, A. V., 2015) (See Fig. S7) with high nitrogen uptake at
344 low relative pressure ($P/P_0 < 0.01$); a feature that is characteristic of microporous materials
345 (Choi et al., 2019). The widening of the knee of the isotherm in sample IV-N indicates a slight
346 broadening of the micropore size range. The pore size distributions illustrate the higher
347 micropore volume in the range of 0.33 to 0.44 nm and a small portion of 1.3 and 1.8 nm pores.
348 The widening of the pore distribution in sample IV-N may be related to the controlled
349 gasification of this particular biochar during pyrolysis at 6 min and 300 W. At powers of 400
350 W, a decrease in the textural properties was observed and may be related to the formation of
351 hot spots which could lead to the detriment of pores by collapse of the pore walls (Huang et
352 al., 2015).

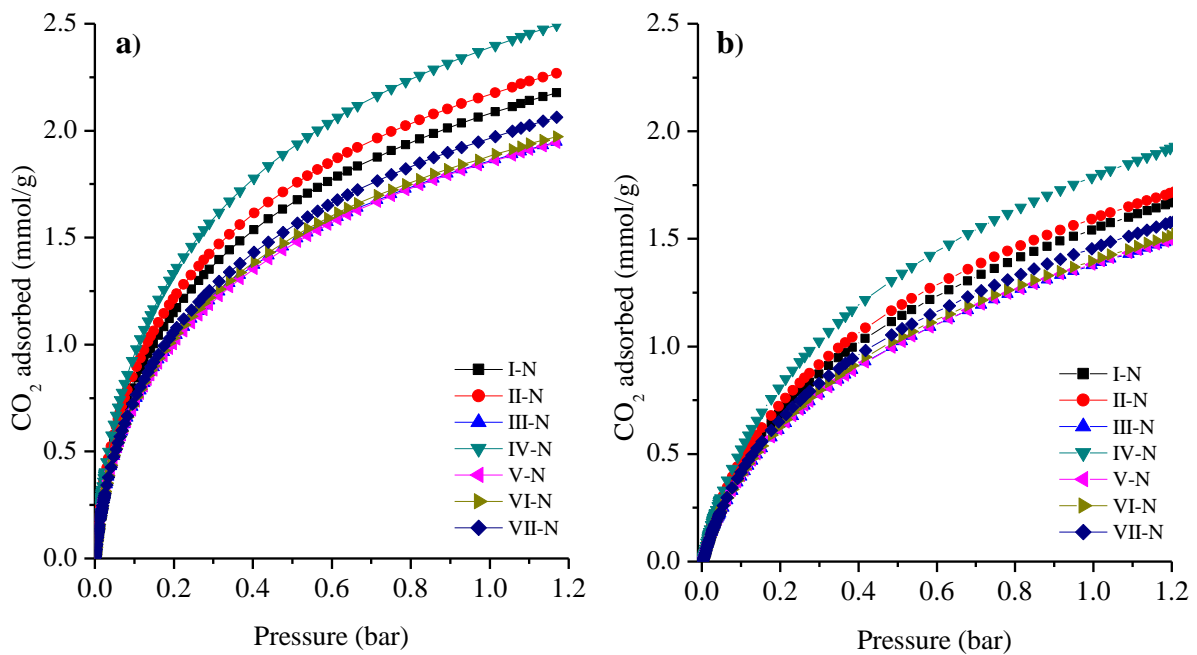
353 **3.4 Evaluation of biochar properties for CO₂ capture**

354 The CO₂ uptake of the biochar produced was explored by volumetric analysis at 0 and 25 °C
355 (Fig. 4). The simple-to-produce biochar in this study, present moderate CO₂ adsorption
356 capacity at atmospheric pressure. The highest adsorption capacity of 2.5 and 2 mmol g⁻¹ at 0
357 and 25 °C, respectively (Fig. 4) was obtained by the biochar (IV-N) produced at 300 W for 6
358 min of microwave heating making it superior to previously published biochars (Table S2,
359 atmospheric pressure), such as rice straw (1.75 mmol g⁻¹) (Huang et al., 2015), sugar cane
360 bagasse and hickory wood (1.67 & 1.32 mmol g⁻¹) (Creamer et al., 2014), walnut shell (1.65
361 mmol g⁻¹) (Lahijani et al., 2018), hickory chips (1.10 mmol g⁻¹) (Xu et al., 2019), pig manure
362 and wheat straw (0.53 & 0.78 mmol g⁻¹) (Xu et al., 2016), mesquite wood and manure chicken
363 (1.92 & 1.60 mmol g⁻¹) (Dissanayake et al., 2020).

364 The CO₂ adsorption results also indicate that biochars have higher CO₂ adsorption capacities
365 than some activated carbons such as oil palm shell activated carbon (1.7 mmol g⁻¹)

366 (Hoseinzadeh Hesas et al., 2015), pitch activated carbon (1.93 mmol g^{-1}) (Lee et al., 2014),
 367 olive stone activated carbon ($1.40 - 1.98 \text{ mmol g}^{-1}$) (Plaza et al., 2014), soybean straw activated
 368 biochar with $\text{CO}_2\text{-NH}_3$ (1.86 mmol g^{-1}) (X. Zhang et al., 2016) and a number of metal organic
 369 frameworks materials, such as MIL-101(Cr) (1.98 mmol/g) (Lin et al., 2014). It is important to
 370 note the advanced materials such as activated carbons, have been reported to have higher CO_2
 371 adsorption capacity, however biochars produced in this study were obtained without employing
 372 additional chemicals for doping or/and activation. This represents a potential alternative due to
 373 their effectiveness, eco-friendly nature, low cost and simple preparation.

374



375

376 Fig. 4. CO_2 uptake at 0 (a) and 25°C (b) for biochars generated without activation from the
 377 microwave pyrolysis

378

Table 2. Elemental composition, proximate analysis and textural parameters of biochars obtained from microwave pyrolysis.

379

Sample	Parameter (%)									Textural parameters			
	C	H	N	^a O	H/C	Moisture	Volatile Matter	Fixed Carbon	Ash	^b S _{BET} (m ² /g)	^c V _p (cm ³ /g)	^d V _{mic} (cm ³ /g)	V _{mes} (cm ³ /g)
I-N [300-3]	83.10	0.89	0.62	15.40	0.011	6.3	12.4	77.5	3.8	122	0.051	0.042	0.009
II-N [300-4]	86.58	0.83	0.80	11.79	0.010	5.2	8.6	82.4	3.7	151	0.062	0.05	0.012
III-N [300-5]	89.84	0.20	0.88	9.08	0.002	6.2	6.7	84.2	3.0	115	0.05	0.039	0.01
IV-N [300-6]	87.41	0.66	0.85	11.08	0.008	5.1	9.4	82.0	3.5	187	0.075	0.066	0.009
V-N [400-2]	83.56	0.99	0.51	14.94	0.012	6.0	7.1	84.2	2.8	42	0.02	0.017	0.003
VI-N [400-3]	87.1	0.37	0.82	11.71	0.004	4.7	9.0	82.5	3.7	134	0.057	0.047	0.01
VII-N [400-4]	91.27	0.12	0.97	7.64	0.001	4.1	6.1	86.6	3.3	112	0.048	0.038	0.01
NS	47.27	6.41	0.18	46.14	0.136	3.6	84.4	10.8	1.3	-	-	-	-

380

Preparation conditions [Power (W)-time (min)]

381

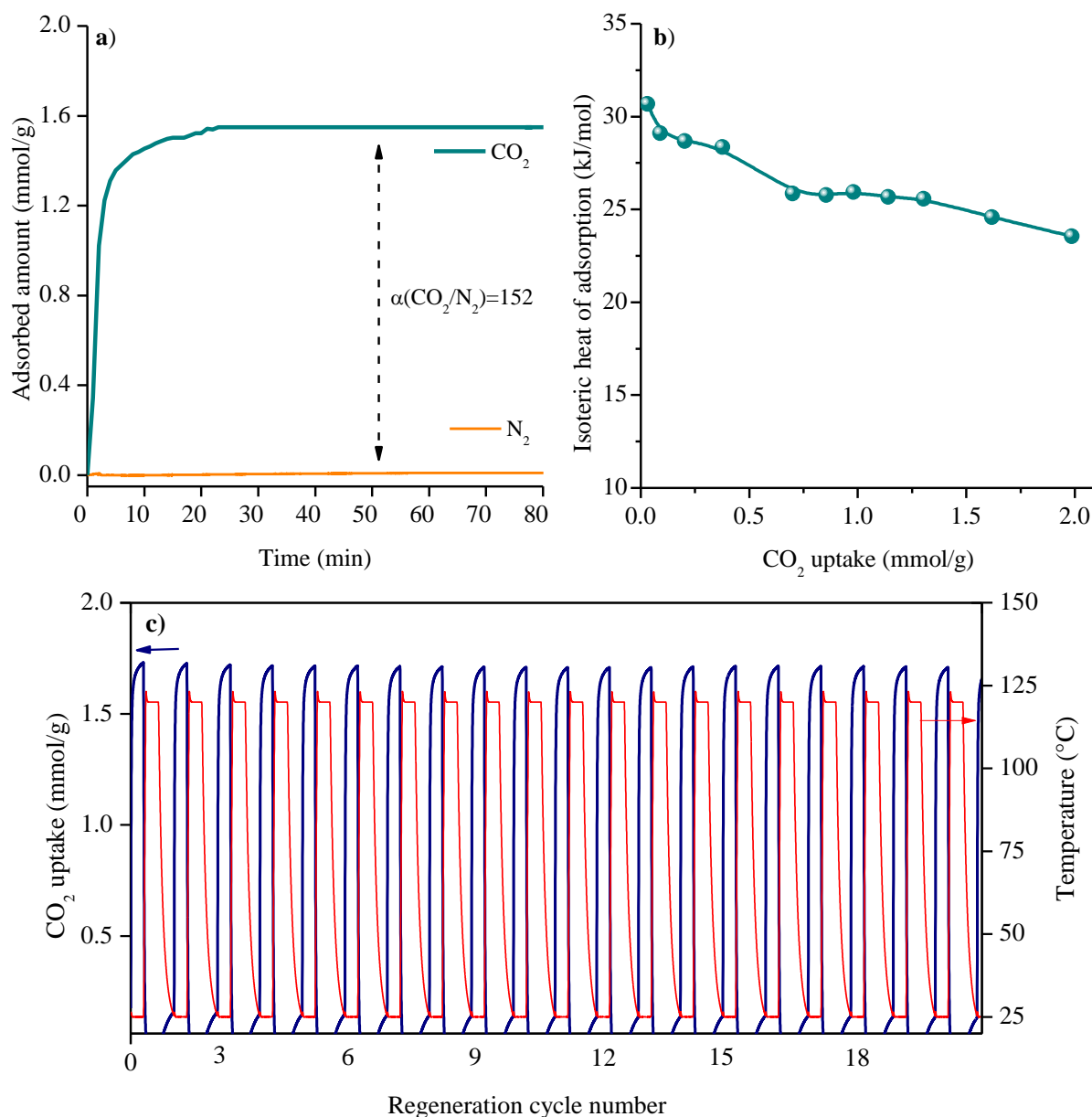
^a Calculated by difference (%O=100-%C-%N-%H)

382

^b BET surface area calculated by the BET method.^c Total pore volume recorded at 100 nm on cumulative pore volume by NLDFT carbon slit pore model.^d Micropore volume obtained at 2 nm on cumulative pore volume by NLDFT carbon slit pore model.

383 The CO₂ uptake capacity was correlated to the higher specific surface area and micropore
384 volume. In our previous study, it was demonstrated that at pressures below to 1 bar, the CO₂
385 uptake is highly controlled by micropores with size below 0.7 nm (Durán-Jiménez et al., 2020).
386 The results this work are also in agreement with the work published by Presser et al. (Presser
387 et al., 2011) where was found that high surface area ($> 2900 \text{ m}^2 \text{ g}^{-1}$) with large total pore volume
388 ($> 1.5 \text{ cm}^3 \text{ g}^{-1}$) is negligible for high CO₂ uptake and that high CO₂ adsorption will result in
389 adsorbents with large narrow micropore volume. These findings are in correlation with the
390 results shown in Fig. S8 that indicate the highest fraction of CO₂ filled pore occurs in pores of
391 size of 0.7 nm, without further uptake increment for pores with size beyond 0.8 nm. This study
392 confirms that pores larger than three times the molecular diameter of CO₂ (i.e. mesoporous
393 materials) does not govern the CO₂ uptake at pre combustion conditions. The correlation of
394 adsorbed amount with narrow micropores is fundamental in the design of effective and un-
395 expensive adsorbents for industrial applications. Additionally, it is well-known the control of
396 narrow micropores can be favourable to increase the CO₂ kinetics. This attribute in adsorbents
397 is highly desirable for practical applications to reduce the required time of contact and energy
398 for regeneration. Fig. 5 (a) presents the adsorption kinetics of biochar IV-N at 25 °C. It shows
399 that levels of CO₂ adsorption up to 90 % can be achieved in less than 10 min, and fully
400 equilibrate after 25 min.

401 To explore the potential of biochar for industrial applications, not only do the CO₂ uptake
402 kinetics and mechanisms need to be considered, but also the CO₂ over N₂ selectivity, the
403 isosteric heat of adsorption, adsorbent stability and recyclability ought to be investigated. The
404 adsorbent's selectivity determines if the CO₂ can be removed from the flue gas mixture with
405 minimal interference from other major gaseous species. In this study the selectivity of sample
406 IV-N for CO₂ over N₂ was determined by thermogravimetric single component analysis at 25
407 °C at 1 bar (Durán-Jiménez et al., 2020). The CO₂ and N₂ uptake are compared in Fig. 5 (a).



408

409 Fig. 5. CO₂ uptake kinetics & gas selectivity of biochar IV-N (a), Isoteric heat (Q_{st}) of CO₂

410 adsorption (b) and recyclability after 20 cycles of CO₂ IV-N at 25 °C (c)

411 The CO₂ uptake of IV-N (1.5 mmol g⁻¹) is distinctive higher than that of N₂ (0.001 mmol g⁻¹).

412 The selectivity based on physisorption uptake, is dependent upon the different physical

413 properties of gas molecules (Parshetti et al., 2015). Since the polarisability of CO₂ is higher

414 than N₂, it is expected to have higher enthalpy of adsorption which leads to a higher affinity of

415 the pore surface, and therefore a higher selectivity. It should also be noted that the selectivity

416 reported in this study is higher than recently reported porous carbon materials (Li and Xiao,
417 2019)(Lahijani et al., 2018)(Chen et al., 2018), indicating that the biochar produced in this
418 study could be implemented for gas separation in practical applications.

419 The high CO₂/N₂ selectivity of IV-N is also supported by the high isosteric heats of adsorption
420 shown in Fig. 5 (b) calculated applying the Clausius-Clapeyron equation (Durán-Jiménez et
421 al., 2020). The relatively high initial Q_{st} values in the low-pressure region, suggest the CO₂
422 molecules are being adsorbed on sites with the highest energy and narrowest micropores. At
423 higher CO₂ uptake, the Q_{st} values decay below 30 kJ mol⁻¹ indicating the CO₂ adsorption is
424 governed by the physisorption mechanism. The values reported for sample IV-N are similar to
425 values reported for porous carbon materials (Chen et al., 2018) (Hong et al., 2016).

426 It is essential to evaluate the regeneration and reusability of the adsorbents to assess its further
427 industrial implementation. Fig. 5c) shows the CO₂ adsorption - desorption cycles of the IV-N
428 biochar at 100 % CO₂. It can be seen that after twenty consecutive cycles the CO₂ adsorption
429 kinetics and equilibrium uptake remained unaffected, confirming the stability and easy
430 regeneration. This result demonstrates the high chemical and physical stability of biochar and
431 confirms the adsorption is reversible governed by mechanisms of the physi-sorption.

432 **4 Conclusions**

433 This work has demonstrated that a range of desirable bio-products with further applications
434 can be effectively synthesised from pecan NS waste biomass employing only 6 min of
435 microwave heating. The yields of the pyrolysis products were found to be greatly influenced
436 by microwave energy and processing parameters, and 8 kJ g⁻¹ of energy was required to obtain
437 39 % of bio-oil that contains upgradeable chemical compounds such as levoglucosan, phenols,
438 and furfural. The results also revealed unique characteristics of the generated biochars, such as
439 pore size distribution and ultra-micropores being the main responsible parameter for the post-

440 combustion CO₂ uptake. The values reported herein (2.5 mmol CO₂ g⁻¹) are competitive or
441 higher than other values reported for other biochars, which include: significantly greater CO₂
442 uptake over N₂ and easy regeneration. These findings are of significant importance, not only
443 due to the competitive properties of biochar and due to its application in the CO₂ capture, but
444 also because it offers a greener and simple approach using microwave heating. Furthermore,
445 no doping agents were used in the synthesis methodology that was employed, making it a great
446 sustainable alternative for waste disposal.

447 **Acknowledgements**

448 This research was supported by the Council of Science and Technology (CONACyT), Mexico
449 under the grant 389535.

450 **5 References**

451 Acevedo-García, V., Rosales, E., Puga, A., Pazos, M., Sanromán, M.A., 2020. Synthesis and
452 use of efficient adsorbents under the principles of circular economy: Waste valorisation
453 and electroadvanced oxidation process regeneration. *Sep. Purif. Technol.* 242, 116796.
454 <https://doi.org/10.1016/j.seppur.2020.116796>

455 Adeniran, B., Masika, E., Mokaya, R., 2014. A family of microporous carbons prepared via a
456 simple metal salt carbonization route with high selectivity for exceptional gravimetric
457 and volumetric post-combustion CO₂ capture. *J. Mater. Chem. A* 2, 14696–14710.
458 <https://doi.org/10.1039/c4ta03565h>

459 Agustin-Salazar, S., Cerruti, P., Medina-Juárez, L.Á., Scarinzi, G., Malinconico, M., Soto-
460 Valdez, H., Gamez-Meza, N., 2018. Lignin and holocellulose from pecan nutshell as
461 reinforcing fillers in poly (lactic acid) biocomposites. *Int. J. Biol. Macromol.* 115, 727–
462 736. <https://doi.org/10.1016/j.ijbiomac.2018.04.120>

463 Aldana, H., Lozano, F.J., Acevedo, J., Mendoza, A., 2015. Thermogravimetric
464 characterization and gasification of pecan nut shells. *Bioresour. Technol.* 198, 634–641.
465 <https://doi.org/10.1016/j.biortech.2015.09.069>

466 Almustapha, M.N., Farooq, M., Andresen, J.M., 2017. Sulphated zirconia catalysed
467 conversion of high density polyethylene to value-added products using a fixed-bed
468 reactor. *J. Anal. Appl. Pyrolysis* 125, 296–303.
469 <https://doi.org/10.1016/j.jaap.2017.03.013>

- 470 Beneroso, D., Monti, T., Kostas, E.T., Robinson, J., 2017. Microwave pyrolysis of biomass
471 for bio-oil production: Scalable processing concepts. *Chem. Eng. J.* 316, 481–498.
472 <https://doi.org/10.1016/j.cej.2017.01.130>
- 473 Bui Viet, D., Chan, W.P., Phua, Z.H., Ebrahimi, A., Abbas, A., Lisak, G., 2020. The use of
474 fly ashes from waste-to-energy processes as mineral CO₂ sequesters and supplementary
475 cementitious materials. *J. Hazard. Mater.* 398, 122906.
476 <https://doi.org/10.1016/j.jhazmat.2020.122906>
- 477 Chen, C., Huang, H., Yu, Y., Shi, J., He, C., Albilali, R., Pan, H., 2018. Template-free
478 synthesis of hierarchical porous carbon with controlled morphology for CO₂ efficient
479 capture. *Chem. Eng. J.* 353, 584–594. <https://doi.org/10.1016/j.cej.2018.07.161>
- 480 Choi, S.W., Tang, J., Pol, V.G., Lee, K.B., 2019. Pollen-derived porous carbon by KOH
481 activation: Effect of physicochemical structure on CO₂ adsorption. *J. CO₂ Util.* 29,
482 146–155. <https://doi.org/10.1016/j.jcou.2018.12.005>
- 483 Coromina, H.M., Walsh, D.A., Mokaya, R., 2015. Biomass-derived activated carbon with
484 simultaneously enhanced CO₂ uptake for both pre and post combustion capture
485 applications. *J. Mater. Chem. A* 4, 280–289. <https://doi.org/10.1039/c5ta09202g>
- 486 Creamer, A.E., Gao, B., Zhang, M., 2014. Carbon dioxide capture using biochar produced
487 from sugarcane bagasse and hickory wood. *Chem. Eng. J.* 249, 174–179.
488 <https://doi.org/10.1016/j.cej.2014.03.105>
- 489 Dissanayake, P.D., Choi, S.W., Igalavithana, A.D., Yang, X., Tsang, D.C.W., Wang, C.H.,
490 Kua, H.W., Lee, K.B., Ok, Y.S., 2020. Sustainable gasification biochar as a high
491 efficiency adsorbent for CO₂ capture: A facile method to designer biochar fabrication.
492 *Renew. Sustain. Energy Rev.* 124, 109785. <https://doi.org/10.1016/j.rser.2020.109785>
- 493 Donahue, C.J., Rais, E.A., 2009. Proximate Analysis of *Leucaena Leucocephala* (Lam.) De
494 Wit, *Parkia Biglobosa* (Jacq.) Benth and *Prosopis Africana* (Guill & Perr.) Taub. *J.*
495 *Chem. Educ.* 86, 222. <https://doi.org/10.1021/ed086p222>
- 496 Durán-Jiménez, G., Hernández-Montoya, V., Montes-Morán, M.A., Rangel-Méndez, J.R.,
497 Tovar-Gómez, R., 2016. Study of the adsorption-desorption of Cu²⁺, Cd²⁺ and Zn²⁺
498 in single and binary aqueous solutions using oxygenated carbons prepared by
499 Microwave Technology. *J. Mol. Liq.* 220, 855–864.
500 <https://doi.org/10.1016/j.molliq.2016.05.027>
- 501 Durán-Jiménez, G., Hernández-Montoya, V., Montes-Morán, M.A., Teutli-León, M., 2015.
502 New oxygenated carbonaceous adsorbents prepared by combined radiant/microwave
503 heating for the removal of Pb²⁺ in aqueous solution. *J. Anal. Appl. Pyrolysis* 113, 599–
504 605. <https://doi.org/10.1016/j.jaap.2015.04.001>
- 505 Durán-Jiménez, G., Monti, T., Titman, J.J., Hernandez-Montoya, V., Kingman, S.W., Binner,
506 E.R., 2017. New insights into microwave pyrolysis of biomass: Preparation of carbon-

- 507 based products from pecan nutshells and their application in wastewater treatment. *J.*
508 *Anal. Appl. Pyrolysis* 124, 113–121. <https://doi.org/10.1016/j.jaap.2017.02.013>
- 509 Durán-Jiménez, G., Stevens, L.A., Kostas, E.T., Hernández-Montoya, V., Robinson, J.P.,
510 Binner, E.R., 2020. Rapid, simple and sustainable synthesis of ultra-microporous
511 carbons with high performance for CO₂ uptake, via microwave heating. *Chem. Eng. J.*
512 388, 124309. <https://doi.org/10.1016/j.cej.2020.124309>
- 513 Ferrera-Lorenzo, N., Fuente, E., Suárez-Ruiz, I., Gil, R.R., Ruiz, B., 2014. Pyrolysis
514 characteristics of a macroalgae solid waste generated by the industrial production of
515 Agar–Agar. *J. Anal. Appl. Pyrolysis* 105, 209–216.
- 516 Haeldermans, T., Claesen, J., Maggen, J., Carleer, R., Yperman, J., Adriaensens, P., Samyn,
517 P., Vandamme, D., Cuypers, A., Vanreppelen, K., Schreurs, S., 2019. Microwave
518 assisted and conventional pyrolysis of MDF – Characterization of the produced
519 biochars. *J. Anal. Appl. Pyrolysis* 138, 218–230.
520 <https://doi.org/10.1016/j.jaap.2018.12.027>
- 521 Hong, S.M., Choi, S.W., Kim, S.H., Lee, K.B., 2016. Porous carbon based on polyvinylidene
522 fluoride: Enhancement of CO₂ adsorption by physical activation. *Carbon N. Y.* 99, 354–
523 360. <https://doi.org/10.1016/j.carbon.2015.12.012>
- 524 Hoseinzadeh Hesas, R., Arami-Niya, A., Wan Daud, W.M.A., Sahu, J.N., 2015. Microwave-
525 assisted production of activated carbons from oil palm shell in the presence of CO₂ or
526 N₂ for CO₂ adsorption. *J. Ind. Eng. Chem.* 24, 196–205.
527 <https://doi.org/10.1016/j.jiec.2014.09.029>
- 528 Huang, Y.F., Chiueh, P. Te, Shih, C.H., Lo, S.L., Sun, L., Zhong, Y., Qiu, C., 2015.
529 Microwave pyrolysis of rice straw to produce biochar as an adsorbent for CO₂ capture.
530 *Energy* 84, 75–82. <https://doi.org/10.1016/j.energy.2015.02.026>
- 531 Jung, S., Park, Y.K., Kwon, E.E., 2019. Strategic use of biochar for CO₂ capture and
532 sequestration. *J. CO₂ Util.* 32, 128–139. <https://doi.org/10.1016/j.jcou.2019.04.012>
- 533 Kan, T., Strezov, V., Evans, T.J., 2016. Lignocellulosic biomass pyrolysis: A review of
534 product properties and effects of pyrolysis parameters. *Renew. Sustain. Energy Rev.* 57,
535 1126–1140. <https://doi.org/10.1016/j.rser.2015.12.185>
- 536 Kostas, E.T., Beneroso, D., Robinson, J.P., 2017. The application of microwave heating in
537 bioenergy: A review on the microwave pre-treatment and upgrading technologies for
538 biomass. *Renew. Sustain. Energy Rev.* 77, 12–27.
539 <https://doi.org/10.1016/j.rser.2017.03.135>
- 540 Kostas, E.T., Durán-Jiménez, G., Shepherd, B.J., Meredith, W., Stevens, L.A., Williams,
541 O.S.A., Lye, G.J., Robinson, J.P., 2020. Microwave pyrolysis of olive pomace for bio-
542 oil and bio-char production. *Chem. Eng. J.* 387, 123404.
543 <https://doi.org/10.1016/j.cej.2019.123404>

- 544 Kostas, E.T., Williams, O.S.A., Duran-Jimenez, G., Tapper, A.J., Cooper, M., Meehan, R.,
545 Robinson, J.P., 2019. Microwave pyrolysis of *Laminaria digitata* to produce unique
546 seaweed-derived bio-oils. *Biomass and Bioenergy* 125, 41–49.
547 <https://doi.org/10.1016/j.biombioe.2019.04.006>
- 548 Lahijani, P., Mohammadi, M., Mohamed, A.R., 2018. Metal incorporated biochar as a
549 potential adsorbent for high capacity CO₂ capture at ambient condition. *J. CO₂ Util.* 26,
550 281–293. <https://doi.org/10.1016/j.jcou.2018.05.018>
- 551 Lee, S.Y., Yoo, H.M., Park, S.W., Hee Park, S., Oh, Y.S., Rhee, K.Y., Park, S.J., 2014.
552 Preparation and characterization of pitch-based nanoporous carbons for improving CO₂
553 capture. *J. Solid State Chem.* 215, 201–205. <https://doi.org/10.1016/j.jssc.2014.03.038>
- 554 Li, J., Dai, J., Liu, G., Zhang, H., Gao, Z., Fu, J., He, Y., Huang, Y., 2016. Biochar from
555 microwave pyrolysis of biomass: A review. *Biomass and Bioenergy* 94, 228–244.
556 <https://doi.org/10.1016/j.biombioe.2016.09.010>
- 557 Li, M., Xiao, R., 2019. Preparation of a dual Pore Structure Activated Carbon from Rice
558 Husk Char as an Adsorbent for CO₂ Capture. *Fuel Process. Technol.* 186, 35–39.
559 <https://doi.org/10.1016/j.fuproc.2018.12.015>
- 560 Li, W., Dang, Q., Brown, R.C., Laird, D., Wright, M.M., 2017. The impacts of biomass
561 properties on pyrolysis yields, economic and environmental performance of the
562 pyrolysis-bioenergy-biochar platform to carbon negative energy. *Bioresour. Technol.*
563 241, 959–968. <https://doi.org/10.1016/j.biortech.2017.06.049>
- 564 Li, Y., Ruan, G., Jalilov, A.S., Tarkunde, Y.R., Fei, H., Tour, J.M., 2016. Biochar as a
565 renewable source for high-performance CO₂ sorbent. *Carbon N. Y.* 107, 344–351.
566 <https://doi.org/10.1016/j.carbon.2016.06.010>
- 567 Liang, Z., Marshall, M., Chaffee, A.L., 2009. CO₂ adsorption-based separation by metal
568 organic framework (Cu-BTC) versus zeolite (13X). *Energy and Fuels* 23, 2785–2789.
569 <https://doi.org/10.1021/ef800938e>
- 570 Lin, Y., Lin, H., Wang, H., Suo, Y., Li, B., Kong, C., Chen, L., 2014. Enhanced selective
571 CO₂ adsorption on polyamine/MIL-101(Cr) composites. *J. Mater. Chem. A* 2, 14658–
572 14665. <https://doi.org/10.1039/c4ta01174k>
- 573 Lozano, F.J., Lozano, R., 2018. Assessing the potential sustainability benefits of agricultural
574 residues: Biomass conversion to syngas for energy generation or to chemicals
575 production. *J. Clean. Prod.* 172, 4162–4169.
576 <https://doi.org/10.1016/j.jclepro.2017.01.037>
- 577 Mamaeva, A., Tahmasebi, A., Tian, L., Yu, J., 2016. Microwave-assisted catalytic pyrolysis
578 of lignocellulosic biomass for production of phenolic-rich bio-oil. *Bioresour. Technol.*
579 211, 382–389. <https://doi.org/10.1016/j.biortech.2016.03.120>

- 580 Martínez-Casillas, D.C., Mascorro-Gutiérrez, I., Arreola-Ramos, C.E., Villafán-Vidales, H.I.,
581 Arancibia-Bulnes, C.A., Ramos-Sánchez, V.H., Cuentas-Gallegos, A.K., 2019. A
582 sustainable approach to produce activated carbons from pecan nutshell waste for
583 environmentally friendly supercapacitors. *Carbon N. Y.* 148, 403–412.
584 <https://doi.org/10.1016/j.carbon.2019.04.017>
- 585 Miura, M., Kaga, H., Sakurai, A., Kakuchi, T., Takahashi, K., 2004. Rapid pyrolysis of wood
586 block by microwave heating. *J. Anal. Appl. Pyrolysis* 71, 187–199.
587 [https://doi.org/10.1016/S0165-2370\(03\)00087-1](https://doi.org/10.1016/S0165-2370(03)00087-1)
- 588 Mohan, D., Pittman, C.U., Steele, P.H., 2006. Pyrolysis of wood/biomass for bio-oil: A
589 critical review. *Energy and Fuels* 20, 848–889. <https://doi.org/10.1021/ef0502397>
- 590 Nagahata, R., Takeuchi, K., 2019. Encouragements for the Use of Microwaves in Industrial
591 Chemistry. *Chem. Rec.* 19, 51–64. <https://doi.org/10.1002/tcr.201800064>
- 592 Namazi, A.B., Allen, D.G., Jia, C.Q., 2015. Probing microwave heating of lignocellulosic
593 biomasses. *J. Anal. Appl. Pyrolysis* 112, 121–128.
594 <https://doi.org/10.1016/j.jaap.2015.02.009>
- 595 Nations, U. Paris Agreement to the United Nations Framework Convention on Climate
596 Change, 2015.
- 597 Olabi, A.G., 2019. Circular economy and renewable energy. *Energy* 181, 450–454.
598 <https://doi.org/10.1016/j.energy.2019.05.196>
- 599 Parshetti, G.K., Chowdhury, S., Balasubramanian, R., 2015. Biomass derived low-cost
600 microporous adsorbents for efficient CO₂ capture. *Fuel* 148, 246–254.
601 <https://doi.org/10.1016/j.fuel.2015.01.032>
- 602 Pinheiro Pires, A.P., Arauzo, J., Fonts, I., Domine, M.E., Fernández Arroyo, A., Garcia-
603 Perez, M.E., Montoya, J., Chejne, F., Pfromm, P., Garcia-Perez, M., 2019. Challenges
604 and opportunities for bio-oil refining: A review. *Energy and Fuels* 33, 4683–4720.
605 <https://doi.org/10.1021/acs.energyfuels.9b00039>
- 606 Plaza, M.G., González, A.S., Pis, J.J., Rubiera, F., Pevida, C., 2014. Production of
607 microporous biochars by single-step oxidation: Effect of activation conditions on CO₂
608 capture. *Appl. Energy* 114, 551–562. <https://doi.org/10.1016/j.apenergy.2013.09.058>
- 609 Presser, V., McDonough, J., Yeon, S., Gogotsi, Y., 2011. Effect of pore size on carbon
610 dioxide sorption by carbide derived carbon. *Energy Environ. Sci.* 3059–3066.
611 <https://doi.org/10.1039/c1ee01176f>
- 612 Rover, M.R., Aui, A., Wright, M.M., Smith, R.G., Brown, R.C., 2019. Production and
613 purification of crystallized levoglucosan from pyrolysis of lignocellulosic biomass.
614 *Green Chem.* 21, 5980–5989. <https://doi.org/10.1039/c9gc02461a>

- 615 Saha, D., Bao, Z., Jia, F., Deng, S., 2010. Adsorption of CO₂, CH₄, N₂O, and N₂ on MOF-
616 5, MOF-177, and zeolite 5A. *Environ. Sci. Technol.* 44, 1820–1826.
617 <https://doi.org/10.1021/es9032309>
- 618 Sanna, A., Dri, M., Hall, M.R., Maroto-Valer, M., 2012. Waste materials for carbon capture
619 and storage by mineralisation (CCSM) - A UK perspective. *Appl. Energy* 99, 545–554.
620 <https://doi.org/10.1016/j.apenergy.2012.06.049>
- 621 Santos, M.S.N. do., Zobot, G.L., Mazutti, M.A., Ugalde, G.A., Rezzadori, K., Tres, M. V.,
622 2020. Optimization of subcritical water hydrolysis of pecan wastes biomasses in a semi-
623 continuous mode. *Bioresour. Technol.* 306, 123129.
624 <https://doi.org/10.1016/j.biortech.2020.123129>
- 625 Sears, K.E., Behringer, R.R., Rasweiler, J.J. 4th, Niswander, L.A., 2006. Development of bat
626 flight: morphologic and molecular evolution of bat wing digits. *Proc. Natl. Acad. Sci. U.*
627 *S. A.* 103, 6581–6586. <https://doi.org/10.1073/pnas.0509716103>
- 628 Serafin, J., Baca, M., Biegun, M., Mijowska, E., Kaleńczuk, R.J., Sreńscek-Nazzal, J.,
629 Michalkiewicz, B., 2019. Direct conversion of biomass to nanoporous activated
630 biocarbons for high CO₂ adsorption and supercapacitor applications. *Appl. Surf. Sci.*
631 497. <https://doi.org/10.1016/j.apsusc.2019.143722>
- 632 Singh, G., Lakhi, K.S., Sil, S., Bhosale, S. V., Kim, I.Y., Albahily, K., Vinu, A., 2019.
633 Biomass derived porous carbon for CO₂ capture. *Carbon N. Y.* 148, 164–186.
634 <https://doi.org/10.1016/j.carbon.2019.03.050>
- 635 Srinivas, G., Krungleviciute, V., Guo, Z.X., Yildirim, T., 2014. Exceptional CO₂ capture in a
636 hierarchically porous carbon with simultaneous high surface area and pore volume.
637 *Energy Environ. Sci.* 7, 335–342. <https://doi.org/10.1039/c3ee42918k>
- 638 Thommes, M., Kaneko, K., Neimark, A. V., et al., 2015. Physisorption of gases, with special
639 reference to the evaluation of surface area and pore size distribution (IUPAC Technical
640 Report).
- 641 Thommes, M., Kaneko, K., Neimark, A. V., Olivier, J.P., Rodriguez-Reinoso, F., Rouquerol,
642 J., Sing, K.S.W., 2015. Physisorption of gases, with special reference to the evaluation
643 of surface area and pore size distribution (IUPAC Technical Report). *Pure Appl. Chem.*
644 87, 1051–1069. <https://doi.org/10.1515/pac-2014-1117>
- 645 Weihong, Z., Bin, B., Guanyi, C., Longlong, M., Beibei, Y., 2019. Thermogravimetric
646 characteristics and kinetics of sawdust pyrolysis catalyzed by potassium salt during the
647 process of hydrogen preparation. *Int. J. Hydrogen Energy* 44, 15863–15870.
648 <https://doi.org/10.1016/j.ijhydene.2019.01.060>
- 649 Wu, Y.M., Zhao, Z.L., Li, H. Bin, He, F., 2009. Low temperature pyrolysis characteristics of
650 major components of biomass. *Ranliao Huaxue Xuebao/Journal Fuel Chem. Technol.*
651 37, 427–432. [https://doi.org/10.1016/s1872-5813\(10\)60002-3](https://doi.org/10.1016/s1872-5813(10)60002-3)

- 652 Xu, X., Kan, Y., Zhao, L., Cao, X., 2016. Chemical transformation of CO₂ during its capture
653 by waste biomass derived biochars. *Environ. Pollut.* 213, 533–540.
654 <https://doi.org/10.1016/j.envpol.2016.03.013>
- 655 Xu, X., Zheng, Y., Gao, B., Cao, X., 2019. N-doped biochar synthesized by a facile ball-
656 milling method for enhanced sorption of CO₂ and reactive red. *Chem. Eng. J.* 368, 564–
657 572. <https://doi.org/10.1016/j.cej.2019.02.165>
- 658 Yang, J., Yue, L., Hu, X., Wang, L., Zhao, Y., Lin, Y., Sun, Y., DaCosta, H., Guo, L., 2017.
659 Efficient CO₂ Capture by Porous Carbons Derived from Coconut Shell. *Energy and*
660 *Fuels* 31, 4287–4293. <https://doi.org/10.1021/acs.energyfuels.7b00633>
- 661 Yin, C., 2012. Microwave-assisted pyrolysis of biomass for liquid biofuels production.
662 *Bioresour. Technol.* 120, 273–284. <https://doi.org/10.1016/j.biortech.2012.06.016>
- 663 Zappa, W., Junginger, M., van den Broek, M., 2019. Is a 100% renewable European power
664 system feasible by 2050? *Appl. Energy* 233–234, 1027–1050.
665 <https://doi.org/10.1016/j.apenergy.2018.08.109>
- 666 Zhang, C., Song, W., Ma, Q., Xie, L., Zhang, X., Guo, H., 2016. Enhancement of CO₂
667 Capture on Biomass-Based Carbon from Black Locust by KOH Activation and
668 Ammonia Modification. *Energy and Fuels* 30, 4181–4190.
669 <https://doi.org/10.1021/acs.energyfuels.5b02764>
- 670 Zhang, X., Wu, J., Yang, H., Shao, J., Wang, X., Chen, Y., Zhang, S., Chen, H., 2016.
671 Preparation of nitrogen-doped microporous modified biochar by high temperature CO₂-
672 NH₃ treatment for CO₂ adsorption: Effects of temperature. *RSC Adv.* 6, 98157–98166.
673 <https://doi.org/10.1039/c6ra23748g>

674